Research Square

Preprints are preliminary reports that have not undergone peer review.
They should not be considered conclusive, used to inform clinical practice,
or referenced by the media as validated information.

Unveiling Structural Versatility and Morphological Tunability of Triple-Phase $CdTiO_3$ Perovskite for High-Performance of p–n Junction Diode

Yogeshwaran A.

yogiphy14@gmail.com

Ramakrishna Mission Vidyalaya

Suresh R

Ramakrishna Mission Vidyalaya

M. Aslam Manthrammel

king Khalid univeristy

Mohd shakir

king Khalid univeristy

Thangabalu S

Saveetha Institute of Medical And Technical Sciences

Research Article

Keywords: Thin film, JNSP, Junction diodes, optoelectronic applications, Photo-diode, Photovoltaic devices

Posted Date: June 18th, 2026

DOI: https://doi.org/10.21203/rs.3.rs-9764406/v1

License: This work is licensed under a Creative Commons Attribution 4.0 International License.
Read Full License

Additional Declarations:
No competing interests reported.

Table 1 to 4 are available in the Supplementary Files section.

Unveiling Structural Versatility and Morphological Tunability of Triple-Phase $CdTiO_3$ Perovskite for High-Performance of p–n Junction Diode

A. Yogeshwaran[a], R. Suresh[a*], M. Aslam Manthrammel[b], Mohd Shkir[b], Thangabalu Subramani[c]

[a] Department of Physics, Sri Ramakrishna Mission Vidyalaya College of Arts and Science, Coimbatore - 641 020, Tamil Nadu, India.

[b] Department of Physics College of Science, King Khalid University, Abha, 61413, 9 Saudi Arabia

[c] Department of Physics, Saveetha School of Engineering, Saveetha Institute of Medical and Technical Science, SIMATS, Chennai – 602 105, Tamil Nadu, India.

*__Corresponding author__: rsdphy@gmail.com **(Dr. R. Suresh)**

Abstract

Highly uniform and well-dispersed cadmium-titanium ($CdTiO_3$) films were successfully deposited using the JNSP technique under varying temperature conditions. $CdTiO_3$ thin films were methodically investigated using XRD, FTIR, SEM, PL, UV-Vis, and I–V characteristics. XRD revealed a rhombohedral crystal structure, with the $CdTiO_3$ perovskite concentration significantly influencing the parameters. FTIR spectroscopy identified the functional groups present in the $CdTiO_3$. Morphological analysis demonstrated the formation of nanoporous structures. Further confirmation of the perovskite structure of $CdTiO_3$ films was achieved through XPS, which verified that the films exhibit a higher oxidation state. Optical studies revealed a bandgap range of 2.68 to 2.53 eV, indicating excellent suitability for higher absorption. The PL spectra displayed strong and broad emission bands at 361 nm and 377 nm, confirming the presence of significant electronic transitions in the material. Current-Voltage (I-V) characteristics exhibit the good conductivity of the thin films at higher temperatures. For $CdTiO_3$/p-Si type p-n junction diodes, the parameters of ideality factor (n) were found to decrease to 12.59, and the barrier height will be 0.415 eV with an increase in temperature. The fabricated device at 450°C shows better results for enhancing the diode parameters and its optoelectronic applications.

Keywords: Thin film; JNSP; Junction diodes; optoelectronic applications; Photo-diode; Photovoltaic devices.

1. Introduction

The recent advancements in optoelectronic devices have indeed shifted focus from traditional organic materials to inorganic alternatives, primarily due to the limitations associated with organic materials, such as their availability and production costs. Inorganic materials, such as metal oxides and perovskites, have gained significant attention for their superior properties, including high stability, excellent charge transport capabilities, and tunable band gaps, making them suitable for various photovoltaic applications [**1**]. Photodiodes, as critical components in optoelectronics, serve the essential function of converting light into electrical current. These photonic components find their use base in solar energy devices and optical communication systems. p-n junction and Schottky photodiodes function based on their combinatory characteristics of optical and electrical behavior. The response efficiency of photodiodes depends strongly on their ability to absorb light and produce electron-hole pairs, as documented in [**2**]. A photodiode subject to illumination creates electron-hole pairs, which form next to its junction interface. The electric field sitting at the junction acts as a key element for charging division, followed by effective charge carrier segmentation within reverse-bias regions. The electric field reaches higher levels of strength within this condition, which allows better collection of charge carriers, thus boosting photocurrent production [**3**]. The diligence to understand photo response behavior in reverse bias helps improve photodiode design because it controls how devices function across UV to visible to infrared wavelength ranges [**4**]. The use of inorganic materials in optoelectronic devices primarily drives photodiode advancement due to their ability to improve both performance sophistication and efficiency levels. The capability of light energy conversion by devices relies on optimized structural and material properties, which can be engineered through careful design methods [**5**].

Semiconductor electrical properties depend heavily on the quantity of impurities because the resulting movement of the Fermi level directly impacts material electrical properties. In semiconductor physics, understanding the Fermi level represents an essential concept because its energy value defines the 50% chance area for electron detection. Semiconductor impurity introduction results in shifts of the Fermi level toward the conduction band when doping produces free electrons or toward the valence band when holes appear. During semiconductor production and post-synthesis diffusion treatments, researchers introduce specific impurities known as dopants into semiconductor materials through controlled processes. Through doping techniques, researchers gain control to modify the electrical as well as optical characteristics of semiconductors to fulfill different application needs. Doping wide bandgap semiconductors achieves substantial electrical conductivity

enhancement alongside modified optical properties, which enables these materials to serve as key elements for diverse advanced technologies, including optoelectronic devices and sensors [**6**]. Cadmium titanium oxide ($CdTiO_3$) stands as the choice material because it possesses essential electrical, optical and mechanical properties that drive high-performance device applications. A wide bandgap in $CdTiO_3$ provides effective light harvesting ability while increasing carrier transport capability. Its wide bandgap signature reduces coupling losses, which proves especially beneficial for optoelectronic applications [**7**]. The tunable characteristics of $CdTiO_3$ become possible through material doping techniques combined with material combinations, which enable applications in photovoltaic cells and photodetectors together with light-emitting diodes (LEDs). Advancements in synthetic methods with sol-gel and spray pyrolysis now enable better control of $CdTiO_3$ film crystallinity and morphology, which produces enhanced device performance [**8**]. Its stable nature, combined with adjustable characteristics to respond to environmental changes, positions $CdTiO_3$ as an optimal choice for stable optoelectronic applications. The analysis investigates $CdTiO_3$ device efficiency improvement through structure-to-property and doping-level assessment of synthesis methods as well as optical and electronic behavior examination. This investigative work showcases the emerging potential of $CdTiO_3$ as an advanced material in optoelectronic applications that fuels upcoming technology developments [**9**].

JNSP operates as an effective and adaptable thin film deposition method used extensively for developing semiconductor components. Precursor solutions prepared specifically undergo atomization to produce extremely fine droplets before the application of elevated temperatures completes the process. A high-quality uniform film develops on the substrate when the droplets go through thermal decomposition while solidifying under these specified conditions. Precise and consistent film deposition plays a vital role in optoelectronics applications, where this procedure demonstrates exceptional value. Fasted and energy-efficient Schottky barrier diodes (SBDs) operate effectively in optoelectronic devices because of their low forward voltage requirements. Device performance of SBDs depends heavily on interface quality between metals and semiconductors because the resulting Schottky barrier height determines device efficiency. With JNSP, researchers gain optimal control over film parameters, including thickness and morphology, and composition, that optimizes diode interfaces for improved SBD performance. [**10**]. This deposition technique presents several advantages in thin-film fabrication: it provides highly uniform coatings over large areas, minimizes material wastage, and allows the incorporation of dopants directly into the film

matrix during the deposition process. Such control and versatility are crucial for achieving desired electrical properties and improving overall device performance [**11**]. Recent studies indicate that JNSP contributes to the formation of films with enhanced crystallinity and reduced defect densities, factors that significantly improve the optoelectronic properties of SBDs. The application of this method to semiconductor thin-film deposition not only enhances device efficiency but also holds promise for advancing the precision and performance of optoelectronic technologies [**12**].

In the present work, thin films were prepared using the JNSP technique for different substrate temperatures (350, 400 & 450). Structural, morphological, optical, elemental, and electrical properties of $CdTiO_3$ thin films were characterized by XRD, FE-SEM, EDX, UV Vis, PL, XPS and I-V characteristics. The p-n junction diode was fabricated using $CdTiO_3$ films at various temperatures. This work presents a feasibility study on the rectification properties of a spray-coated FTO substrate.

2. Experimental Section

The synthesis of perovskite-based cadmium titanium oxide ($CdTiO_3$) films was meticulously carried out using cadmium chloride monohydrate ($CdCl_2 \cdot H_2O$) and titanium trichloride ($TiCl_3$) as precursors, both sourced from reputable suppliers. Cadmium chloride monohydrate, with a molecular weight of 201.33 g/mol, was obtained from Merck (India) Mumbai Limited, while titanium trichloride, available as a ≥12% solution with a molecular weight of 154.23 g/mol, was procured from Otto Chemi Pvt. Ltd. The reagent quantities were precisely calculated to achieve the desired molar concentration of 0.4 M, requiring of $CdCl_2.H_2O$ ensuring accuracy and consistency in the preparation. Precursor solutions underwent dissolution in 20 ml of double-distilled deionized water, then the solution was stirred at 300 rpm for two hours to ensure a homogeneous mixture. This mixture was then evenly divided into two 10 ml portions, which were recombined in a 1:1 ratio. Additional mixing under identical agitation settings occurred throughout the subsequent two hours of synthesis. Proper distribution and cross-species interaction of chemicals were achieved during this processing stage.

A meticulous cleaning approach for FTO substrates improved their capacity to accept thin-film deposits. The substrate preparation involved cleaning 2 cm × 1.5 cm specimens using a Triton X-100 detergent solution, followed by extensive deionized water rinses to remove detergent residue before placing them in isopropyl alcohol for cleaning of organics. Ultrasonic

cleaning followed by deionized water rinses led to substrate purification for placement inside the furnace. A JNSP system deposited $CdTiO_3$ films through furnace annealing at three different temperatures ranging from 350°C to 450°C. The controlled temperature processes functioned as essential elements to maximize both structural and optical features of these films. Thermal management techniques, combined with the uniform application of a precursor solution, resulted in the successful creation of top-quality perovskite thin films on cleaned substrates. **Fig. 1.** Schematic representation of the preparation of $CdTiO_3$ films.

3. Results and Discussion

3.1 Structural analysis

X-ray diffraction (XRD) analysis was conducted using CuKα radiation with a wavelength of 1.5406 Å to examine the crystalline structure of the $CdTiO_3$ films. The XRD results confirmed the triple-phase system rhombohedral, cubic, and tetragonal crystal structure of the films as a phase, as depicted in **Fig. 2a**, and it is well matched with JCPDS card 00-029-0277. Films synthesized at a lower temperature of 350°C exhibited dominant diffraction peaks, particularly at $2\theta = 36.6°$, which displayed high intensity. This increased intensity is attributed to enhanced crystallinity, resulting in well-ordered atomic arrangements that promote stronger constructive interference of X-rays at specific diffraction angles [**13**]. Other observed peaks at 2θ values of 26.8°, 31.5°, and 34.8° correspond to the Miller indices (111), (104), and (110), respectively. These peaks demonstrated relatively lower intensities than the 36.6° peak, likely due to internal stresses or lattice distortions that disrupt atomic periodicity and reduce coherence in scattered X-rays [**14**]. The diffraction patterns displayed substantial modifications with rising synthesis temperature. At $2\theta = 36.1°$, the peak intensity grew stronger because synthesis temperatures enabled better atomic alignment with systematic patterns that decreased defects and minimized lattice strain. Peak intensity analysis showed predominant peaks corresponding to a reduction at 450°C despite the discovery of ascending intensity from peaks representing (104) and (110) crystals [**15**]. Secondary phases alongside reoriented grain formation may explain this transformation, which occurs due to changes in the crystal growth mechanism and probable phase composition redistribution. The scientific observations make clear how synthesis temperature interacts with crystallographic orientation while influencing the phase distribution of $CdTiO_3$ films [**16**]. The conducted research demonstrates essential conditioning of film temperature to control structural as well as optical attributes which qualify these films for electronic and optoelectronic device applications. Different temperatures during

synthesis lead to simultaneous grain enlargement together with phase transitions which eventually creates equilibrium between total magnetic signals that determine final performance outcomes from materials. The crystallite size (D) is calculated by the Debye-Scherrer equation [**17**]

$$D = \frac{K\lambda}{\beta \cos\theta} \qquad (1)$$

where D - crystallite size, λ - wavelength (λ = 0.15418 nm), Scherrer constant (K)=0.89, β - full-width half maximum and θ - diffraction angle. A rise in atomic mobility associated with substrate temperature variations explains why $CdTiO_3$ perovskite films grown on FTO substrates show increasing crystallite sizes from 23.37 to 31.73 nm. This enhanced mobility allows for overcoming energy barriers more effectively and migrating to energetically favorable lattice sites, reducing the defects and promoting larger, more coherent crystallite growth. Higher substrate temperatures favor the formation of thermodynamically stable phases with larger grain sizes. This stability results from the minimization of surface and interfacial energies, which drives the system toward larger crystallites to reduce overall energy.

Micro strain (ε), dislocation density (δ) and stacking fault (SF) are considered by the following formula and the results are placed as revealed in **Table 1.**

$$\delta = \frac{1}{D^2} \qquad (2)$$

$$\varepsilon = \beta \frac{\cos\theta}{4} \qquad (3)$$

$$SF = \left[\frac{2\pi^2}{45(3\tan\theta)^{\frac{1}{2}}}\right]\beta \qquad (4)$$

In $CdTiO_3$ films, the increase in crystallite size with a decrease in microstrain, dislocation density and stacking faults, As the substrate temperature increases, atoms deposited onto the FTO substrate gain sufficient kinetic energy to occupy energetically favorable positions in the crystal lattice. This enhanced atomic mobility reduces lattice defects such as dislocations and stacking faults because the atoms rearrange into a more stable and ordered configuration [**18**]. With fewer defects acting as barriers to crystallite growth, larger crystallites are formed. Increased crystallite size reduces the surface-to-volume ratio, minimizing surface energy and relieving internal stresses. Consequently, microstrain decreases from 0.1898 to

0.1676 x (lines^{-2}m^{-4}) as larger crystallites have more uniform and relaxed atomic arrangements, leading to a more stable crystalline structure [**19**]. Dislocation density decreases from (1.8311 to 0.9931) 10^{-14} (lines cm^{-2}) with increasing crystallite size because larger crystallites inherently contain fewer defects per unit volume. As smaller grains merge during growth, dislocations are annihilated or rearranged into lower-energy configurations, further reducing dislocation density. As substrate temperature rises, the enhanced thermal energy allows atoms to rearrange into proper lattice positions, correcting misalignments in stacking sequences. And its ranges from (0.0398 to 0.0284) x 10^{-2}. The above observative findings of structural analysis of $CdTiO_3$ films with increasing substrate temperature enhance crystallite size while reducing microstrain, dislocation density and stacking faults [**20**]. These improvements minimize defects, optimize charge carrier mobility and increase electrical conductivity, making the films ideal for optoelectronic applications as shown in table 2 Average Crystal Size and Micro strain calculated **Fig. 2b.** 2D counter plot for the sequence of phase transition on the studied temperature range. Due to the obtained thermal dependence of the crystallographic cell structure, which has been analyzed in the XRD patterns as shown in **Fig. 2c. Fig. 3.** shows the structural parameter Vs different substrate temperatures for $CdTiO_3$ films.

3.2. Functional Analysis

The FTIR spectrum of $CdTiO_3$ thin films for different temperatures is shown in **Fig. 4a.** It reveals several distinct peaks corresponding to specific functional groups, providing insights into the compound's chemical structure. The strong and sharp peaks observed wavenumber of 1029.29 cm^{-1} signify C–O stretching vibrations from residual organic precursors or solvents and may also overlap with Ti–O stretching in the $CdTiO_3$ lattice. The peak at 2331.94 cm^{-1} is attributed to stretching vibrations of C≡N bonds, while the 2197.92 cm^{-1} and 2110.19 cm^{-1} bands likely arise from C≡N stretching, indicating nitrile groups. 2032.69 cm^{-1} corresponds to CO_2 stretching vibrations and may be possible carbonate or organic contamination. The 1840.32 cm^{-1} peak might be linked to C=C stretching or ester, carbonyl functional groups, while 1758.05 cm^{-1} and 1652.96 cm^{-1} are characteristic of carbonyl stretching in esters, ketones, or amides [**21**]. The 1515.35 cm^{-1} peak reflects C=C stretching in aromatic compounds and 1440.94 cm^{-1} is attributed to bending vibrations of CH_2 or CH_3 groups in alkyl chains. 1331.16 cm^{-1} indicates N–H bending particularly for amides or amines, and 1228.98 cm^{-1} and 1157.21 cm^{-1} are associated with C–O stretching in ethers or alcohols [**22**]. The 1029.29 cm^{-1} peak corresponds to C–O bending, common in alcohols or ethers, while 992.03 cm^{-1} may be linked to Si–O–Si bending or C–C stretching. Peaks at 882.23 cm^{-1} and

827.20 cm^{-1} are typically associated with C–H bending or Si–O bending, while 737.16 cm^{-1} is likely related to CH_2 or CH_3 bending vibrations. The peaks at 645.26 cm^{-1}, 512.07 cm^{-1} and 426.39 cm^{-1} suggest M–O stretching and bending vibrations, typical of metal-oxide compounds, that the crystallization process is essentially supersaturated at 450°C, as evidenced by the decrease in organic interference peaks. As shown in **Fig. 4b**, due to the resonance peak gradually reducing in the low energy tails, the correlation matrices show primarily small magnitude and short-range positive correlations [**23**]. Consequently, higher temperatures result in dominant intensity peaks with superior vibration and crystalline properties because the FTO film's structural integrity and crystallinity increase with temperature.

3.3. Morphology and elemental analysis

The FE-SEM image of $CdTiO_3$ thin films as shown in **Fig. 5.** demonstrates a heterogeneous texture that reveals regions with varying contrasts, ranging from smoother to rougher surfaces. This variation suggests that the film has a polycrystalline structure it revealing that of multiple small crystal grains. At a temperature of 350°C, the $CdTiO_3$ thin film exhibits a porous and agglomerated structure. Thick, irregularly formed grains along with disorganized surface texture characterize these thin films. The specimen demonstrates poorly defined grain boundaries and substantial porosity between grains at this temperature level [**24**]. A prominent shift in the material's structure becomes apparent when the measurement temperature reaches 400°C. At this temperature level, the crystal structure becomes sharper with reduced openings between grains throughout the film. The sintering process reveals its initial action through the unification of small particles into larger ones. The intermediate temperature stimulates grain growth and coalescence between particles, which results in tighter material structure and a reduction of porosity. At the microstructural level, the film solidifies and develops connected features because of decreased porosity [**25**]. Raising the temperature to 450°C results in a more substantial evolution of the film structure. The material develops an extremely dense microstructure, which shows a robust connection between its components after massive grain enlargement. New shapes and dimensional uniformity in the grains indicate that the sintering advancement has reached a further stage. The grain enhancement at this thermal condition produces a dense microstructure that maintains low porosity. The $CdTiO_3$ thin film shows enhanced grain coalescence behaviour at higher processing temperatures, resulting in improved structural integrity along with a better-quality microstructure.

EDAX spectroscopy performed elemental analyses of $CdTiO_3$ thin films to yield compositional data as samples aged at different temperatures. EDX spectrum shows which elements exist in the sample by presenting both Cd with Ti along with O. Analysis with energy dispersive X-ray (EDAX) detected all fundamental elements Cadmium, Titanium and Oxygen as observed in **Fig. 6.**

3.4. Compositional Analysis

It is a powerful, non-destructive technique that analyses chemical and electronic properties. The XPS survey graph represents the pure $CdTiO_3$ thin film at 450°C as shown in **Fig. 7.** The XPS spectrum examines the electronic and chemical nature of Cd and Ti together with O through their elemental features, which support quantitative analysis and identification. The spin-orbit coupling produced by electron angular momentum and spin interaction results in two peaks labelled Cd $3d_{5/2}$ and Cd $3d_{3/2}$ in the Cd 3d spectrum. This coupling leads to an energy separation of 6.27 eV, a characteristic marker for cadmium, particularly in its Cd^{2+} oxidation state [**26**]. The precise binding energy positions of these peaks can vary slightly based on the chemical environment, with cadmium bonded to electronegative elements like oxygen (CdO) often exhibiting higher binding energies than metallic cadmium (Cd) and the Cd 3p orbital represents the prominent peak are 618.82 eV and satellite peak are 652.72 eV and this coupling leads to an energy separation of 33.9 eV. Furthermore, the Ti 2p peaks are labelled are spectrum displays spinorbit Ti $2p_{3/2}$ and Ti $2p_{1/2}$, sepration on binding energy values are 5.79 eV characteristic of titanium in its common oxidation state of Ti^{4+} [**27**]. For example, in TiO_2, the Ti $2p_{3/2}$ peak appears near 458.5 eV, while reduced oxidation states, such as Ti^{3+} in Ti_2O_3, exhibit lower binding energies. Broadened or asymmetric peaks in the titanium spectrum often indicate mixed oxidation states, surface defects, or interactions with adsorbed species, reflecting the material's complexity. Meanwhile, the O 1s spectrum reveals a prominent peak at 531.76 eV, corresponding to oxygen in a metal-oxide lattice-like TiO_2, where oxygen exists as O^{2-} ions forming strong bonds with metal cations. Shifts in the O 1s peak position indicate different chemical environments, with lattice oxygen typically appearing at lower binding energies (~530–532 eV), while adsorbed species or hydroxyl groups may cause higher binding energies (~532–533 eV) [**28**].

3.5. Optical Analysis

The UV-Vis absorption spectra of $CdTiO_3$ thin films annealed at varying substrate temperatures (350°C, 400°C, and 450°C) provide critical insights into their optical

characteristics and defect-related behaviors, as shown in **Fig. 8.** These temperature-dependent spectra exhibit distinct absorption bands highlighting the interplay between bandgap transitions and defect states, shedding light on the films' electronic structure and crystallinity. The bandgap absorption of $CdTiO_3$ manifests as the major absorption peak around 400 nm while showing valence-to-conduction band electron transitions. The absorption band intensity grows as temperature rises, indicating improved crystalline disorder and elevated electronic states that enable band-to-band transitions. The material's structure, together with its electronic properties, shows direct sensitivity to substrate temperature variations. The material develops an absorption band at 500 nm after defects create states due to oxygen vacancy formations and lattice structural imperfections. Phenomena inside the bandgap form localized energy states that permit photons to accept lower energy. The band intensity increases as substrate temperature rises because high temperatures promote the creation and stabilization of defect states, which are likely caused by structural rearrangements along with thermal impurity movement [**29**]. The introduction of new absorption states around 600 nm becomes visible at 450°C, while additional defect states and impurity levels appear to be induced by high process temperatures. Research based on the positional change of this feature demonstrates that intense annealing treatments create advanced defect states and trapping locations within the active area of the device. The transmittance spectra of $CdTiO_3$ thin films between 350°C and 400°C and 450°C display crucial observations about optical transparency relationships and material bandgap definitions along with defect state variations at different substrate temperature levels. Results demonstrate how annealing temperature alters the crystalline order and structural compatibility, together with the density of defects within the material. The charts in **Fig. 9.** illustrate how the optical properties of $CdTiO_3$ thin films evolve with different annealing temperatures at 350°C, 400°C and 450°C. Semiconductor thin films showcase a standard transmittance reduction with longer wavelengths because of band structure interactions with photons. Heating conditions lead to substantial transmittance reductions in both visible and near-infrared regions because they modify optical density and generate defects [**15**]. Camera measurements show a distinctive 400 nm absorption edge throughout all samples, which relates to their approximately 3.1 eV intrinsic bandgap and makes them ideal for optoelectronic use. At a heat treatment of 350°C the sample achieves its peak transmittance value which corresponds to its superior optical transparency, while a distinct absorption edge suggests a uniform bandgap variation existence of thickness irregularities or interference patterns. The 400°C thin film shows lower transmission rates coupled with a smooth profile, indicating improved crystal structure and decreased scattering incidents at around 400 nm wavelength.

The film treated at 450°C exhibits the lowest transmittance because of an expanded absorption edge and a small absorption peak at 500 nm, which may stem from defects created by high annealing temperatures [**30**]. The bandgap properties and defect-related absorption within the materials control how these absorption characteristics vary. The bandgap initiates electron transitions for photons having energy greater than 3.1 eV, and various defects created by oxygen vacancies and lattice imperfections result in additional sub-bandgap absorption. The heightened crystallinity achievable at higher temperatures enhances bandgap absorption yet also extends defect-life, leading to decreased transmittance at extended wavelengths. Rational optimization of annealing conditions establishes a key mechanism for adjusting optical properties of $CdTiO_3$ thin films with target applications in advanced optoelectronics. [**31**]. The presented graph highlights the variation in bandgap energy values for $CdTiO_3$ thin films at temperatures of 350°C, 400°C, and 450°C, showcasing a distinct trend of decreasing bandgap energy with increasing temperature as shown in **Fig. 10.** The band gap is calculated from the equation below

$$(\alpha h\nu)^{n} = B(h\nu - E_g) \qquad (5)$$

The values α, h, hν, B, Eg represent the absorption coefficient, Planck's constant, Photon energy, constant and bandgap, respectively. The analysis using Tauc's plot revealed descending bandgap energy values from 2.68 eV in films annealed at 350°C down to 2.53 eV at 450°C. The material's structural character alongside its morphological makeup and electronic structure underwent changes because of thermal treatment, resulting in decreased bandgap energy levels. Bandgap and Urbach energy values calculated for all $_{CdTiO3}$ thin films as shown **Table 3.** Several linked factors explain the decrease in bandgap energy observed with increasing annealing temperatures. The distribution of atoms during high-temperature annealing results in larger crystallite size due to improved atomic mobility leading to recrystallization. Increased crystallite sizes lower both the density of scattering centers and defects which otherwise create localized energy states of the bandgap [**32**]. Material transitions into a more standardized electronic band structure because of which the band gap effectively becomes narrower. The film's defect density shows a significant decline when deposition temperatures rise. The crystalline order of thin film layers becomes sharper at elevated temperatures thus leading to decreased quantities of structural defects such as oxygen vacancies along with interstitials and lattice distortions. The introduction of mid-gap states through these defects transforms optical transitions while simultaneously expanding effective bandgap energy. A reduction in defects generates distinct edges for valence and conduction bands which

results in the observed bandgap contraction. The change in $CdTiO_3$ electronic band structure stems from modifications in atomic arrangement, together with bonding environment within the crystalline lattice structure. Better atomic arrangement alongside redistribution during high-temperature processes controls atom orbital interactions while shaping atom hybridization relationships, thus influencing electronic state densities. The structural reorganization modifies band edges as it produces bandgap energy shifts [**33**]. This bandgap energy tuning regime creates significant effects on electrical along with optical properties of $CdTiO_3$ thin films. The observed bandgap reduction in $CdTiO_3$ thin films enables lower-energy photon absorption which extends optical performance span to visible and near-infrared wavelengths. Enhanced light absorption performance remains essential for photodetection systems which use materials for optoelectronic applications. In **Fig.11.** this periodic structure alignment with lower flaw populations leads to superior electronic charge behavior and minimized losses between electrons as shown in **Fig. 12.**

3.6. PL analysis

Topological analysis of annealed $CdTiO_3$ thin films through photoluminescence (PL) spectroscopy became visible in **Fig. 13.** These spectral patterns enable scientists to examine defect patterns and recombination pathways while revealing fundamental optical behaviors of $CdTiO_3$ thin films through different thermal treatment methods. Near-band-edge emission (NBE) produces a prominent PL peak at 361 nm according to the spectra of the sample heated to 350°C. Intrinsic optical transitions between the conduction band and valence band edges produce this peak during free exciton radiative recombination [**34**]. The strong intensity of this peak across lower temperatures supports a defect-free lattice structure where few defective states interfere with recombination events. An increase in annealing temperatures from 400°C to 450°C leads to diminished NBE emission intensity but simultaneously increases the visible defect emission signals in PL measurements. Increasing the annealing temperature leads to the creation of more defect states throughout the $CdTiO_3$ crystal structure [**35**]. The bandgap area of TiO_2 forever becomes enriched with localized energy states because of oxygen vacancies alongside titanium vacancies and interstitial defects. The New defect levels serve as centers where recombination events take place, preventing radiative transitions from the band edge. The temperature-dependent intensity growth of multiple defect-related peaks occurs within the wavelength range of 377 nm to 489 nm at 377 nm, 411 nm, 438 nm, and 489 nm. Research indicates that oxygen vacancies cause the 377 nm defect peak, but titanium vacancies or complex defect clusters produce the 411 nm and 438 nm features [**36**]. Deep-level defects that

form within the bandgap lead to a peak at 489 nm and could stem from defect complexes or structural distortions caused by elevated thermal energy. Temperature-dependent intensification of these defect-related emissions provides evidence to support fundamental defect-state activation and stabilization mechanisms that restructure the material's electronic structure. The evaluation modifications in optical characteristics affect $CdTiO_3$ thin film structures. The combined effect of higher temperatures creates better atomic mobility making crystals more uniform but also generates more defects that degrade optimum luminescence functionality. The recombination activities at defect sites function as non-radiative paths while reducing the radiative recombination rate until the near-band-edge emission fades and defect state emissions gain strength [**37,38**]. Applications require precise temperature optimization because this management controls the balance between maximizing crystallinity while minimizing disorder formation. High luminescence efficiency dependent optoelectronic technology such as light-emitting diodes and laser diodes, requires minimized emissions due to defects for ideal performance.

3.7. DC electrical conductivity of the thin film

The current-voltage (I-V) characteristics of $CdTiO_3$ thin films at varying temperatures as shown in the **Fig.14**. reveal significant insights into their electrical behavior, highlighting a nonlinear conduction mechanism indicative of resistive switching effects. The I-V curves exhibit a progressive increase in current with applied voltage, demonstrating a steepening slope at higher voltages, which underscores the complex nature of the charge transport processes within these thin films. Among the analyzed samples, the film at 450°C exhibits the highest current values, signalling enhanced electrical conductivity compared to films at lower temperatures, such as 350°C and 400°C. This improvement in conductivity range between the (1.20×10^8 to 2.73×10^9) can be primarily attributed to the increased crystallinity achieved at elevated temperatures. Higher thermal energy facilitates better atomic rearrangement, resulting in larger crystallites, reduced grain boundary scattering, and improved charge carrier mobility. While the resistivity also decreased (9.07×10^7) to (4.40×10^8) as shown in **Table 4.** Additionally, the reduction of certain defect states that act as charge carrier traps further contributes to the observed increase in current flow. Despite this enhancement, the nonlinear nature of the I-V characteristics and the presence of hysteresis loops in the curves suggest that the conduction mechanism is not solely governed by classical Ohmic behavior [**39**]. Instead, it likely involves a combination of complex processes. For instance, space-charge-limited conduction (SCLC) may dominate at higher voltage regions, where the injected carriers exceed

the equilibrium carrier concentration, leading to space charge effects. Simultaneously, Poole-Frenkel emission, a mechanism involving field-assisted thermal ionization of trapped charge carriers, may occur due to the presence of defect states within the bandgap as shown in **Fig. 15.** Additionally, trap-assisted tunnelling, where charge carriers traverse through localized energy states within the bandgap, could further contribute to the observed conduction. The hysteresis observed in the I-V curves, especially prominent at higher voltages, points to resistive switching phenomena, which are characteristic of materials with potential for memory and neuromorphic applications. From **Fig. 16.** the behaviour suggests that the electrical conductivity of the films is influenced by reversible changes in the material's defect structure, such as the migration of oxygen vacancies or the formation and rupture of conductive filaments within the material. These processes can lead to bistable resistance states, making $CdTiO_3$ thin films.

3.8. I-V characterization of the p - n junction diode

The current-voltage (I–V) characteristics of a typical J–V plot for the pure $CdTiO_3$/p-Si device, as shown in **Fig. 17.** illustrate the forward bias direction corresponding to the negative Ag-paste (top) electrode of the device. These characteristics can be attributed to the low work function of the Ag-paste, the high work function of the Si electrodes, and the p-type conduction mechanism of the FTO substrate. In **Fig.18.** reveals the rectifying behavior of this heterojunction, with a typical forward-to-reverse current range spanning from -10 to +10 V. The turn-on voltage, which corresponds to the diffusion or built-in potential, represents the potential barrier that carriers must overcome to contribute to the forward current. Structural imperfections at grain boundaries and the interface could lead to a deterioration in the device. The conductivity of the n-$CdTiO_3$ layer primarily arises from oxygen deficiency, whereas in Si, the excess oxygen induces p-type conductivity. The deposition of $CdTiO_3$ on the Si layer in an oxygen-rich ambient may result in the formation of a very thin, mixed intrinsic layer at the n-$CdTiO_3$/p-Si interface. The forward current increases exponentially with voltage, but the reverse bias current exhibits poor saturation at low reverse voltages and increases gradually. According to thermionic emission (TE) theory, the current through a Schottky diode is governed by the energy barrier height and the temperature-dependent carrier dynamics, which influence the overall performance of the heterojunction is given by

$$I = I_0 \left[\exp\left(q(V - IRs)/ nK_BT\right) - 1\right] \quad (6)$$

Here, I_0 represents the reverse saturation current, q denotes the electron charge, V is the applied voltage, n is the ideality factor, K_B is the Boltzmann constant and T is the absolute temperature. The diode's ideality factor n and reverse bias saturation current I_0 can be determined from the slope and intercept of the semi-logarithmic forward bias I–V plot for V >>3kT/q using the relation (6). The values of n and the barrier height Φ_B can then be calculated based on the relationship derived from the thermionic emission theory. This method provides insight into the charge transport mechanisms and the quality of the heterojunction interface, further contributing to the understanding of device performance under varying conditions.

$$\text{Ideality factor (n)} = \frac{q}{K_B T}\frac{dV}{d(\text{In I})} \quad (7)$$

$$\text{barrier height } (\phi_B) = \frac{K_B}{q}\text{In}\left(\frac{AA^*T^2}{I_0}\right) \quad (8)$$

Here, A denotes the effective diode area, and A* represents the effective Richardson constant. Detailed insights into the transport mechanism through inorganic thin films can be obtained by analyzing the forward current density–voltage (I–V) characteristics. For an ideal Schottky contact, the ideality factor n is equal to unity. However, a higher value of the ideality factor, often exceeding unity, can be attributed to the presence of interface states between the metal and the semiconductor. This occurs because an interfacial film of atomic dimensions typically exists between the metal and the semiconductor, affecting the charge transport dynamics and deviating from ideal Schottky behavior. The values of the ideality factor n and the barrier height Φ_B obtained from the I–V characteristics using Equations (7) and (8). The n and Φ_B values range from 17.015 to 12.59 and 0.405 to 0.415 eV, respectively. **Table 5** represents the ideal factor and barrier height of the prepared device at various temperatures. The high values of the ideality factor can be attributed to various factors, including inhomogeneities in the thickness of the inorganic film, nonuniform distribution of interfacial charges, and the influence of series resistance R_S [**40**]. The series resistance is a critical parameter that significantly affects the electrical characteristics of rectifying contacts. Its impact is particularly notable due to the presence of an interfacial layer between the inorganic layer and the semiconductor, which contributes to deviations from ideal forward bias current–voltage I–V behavior. Typically, the forward bias I–V characteristics exhibit linearity on a semi-logarithmic scale at low applied voltages. However, as the applied voltage increases, the effects of series resistance become more pronounced, causing significant deviations from

linearity and affecting the overall device performance. This method allows for the identification of the series resistance from the slope of the plot at higher voltages, where the current primarily flows through the junction, and the shunt resistance from the intercept at lower voltages, where leakage currents dominate. Analyzing the junction resistance in this manner provides a clearer understanding of how these resistances influence the overall electrical performance of the heterojunction device.

4. Conclusion

The study successfully demonstrated the fabrication of highly uniform and well-dispersed $CdTiO_3$ thin films using the JNSP technique, revealing the significant influence of temperature on their structural, optical, elemental and electrical properties. XRD analysis confirmed the three-phase Rhombohedral, Cubic, and Tetragonal of the $CdTiO_3$ perovskite structure, showing that increased temperatures enhance crystallinity and optimize structural parameters such as grain size, microstrain, dislocation density, and stacking faults. FTIR spectroscopy further validated the structural improvements at higher temperatures, identifying functional groups and enhanced structural characteristics. SEM revealed the formation of nanoporous structures composed of interconnected grains, beneficial for electron transport, while XPS analysis confirmed the films' perovskite structure and higher oxidation state. Optical studies showed a bandgap narrowing from 2.68 to 2.53 eV with increasing temperature, indicating superior light absorption capabilities. The PL spectra exhibited strong emission bands at 361 nm and 377 nm, highlighting significant electronic transitions, while I-V measurements demonstrated enhanced conductivity at elevated temperatures. The analysis of $CdTiO_3$/p-Si p-n junction diodes showed an improved ideality factor and barrier height at higher temperatures, achieving optimal values of 12.59 and 0.415 eV, respectively. The device fabricated at 450°C demonstrated superior performance, making it highly suitable for optoelectronic applications, thus underscoring the pivotal role of temperature in optimizing the multifunctional properties of $CdTiO_3$ thin films.

Acknowledgements

The authors extend their appreciation to the Deanship of Research and Graduate Studies at King Khalid University for funding this work through a Large Research Project under grant number RGP.2/4/46.

Declaration of competing interest

The authors declare that they have no known competing financial interests or personal relationships that could have appeared to influence the work reported in this paper.

Funding

Funding associated with this work

References

[1] Z. Chen, Zhenyu Wang, Jintao Wang, Shuming Chen, Buyue Zhang, Ye Li, Long Yuan, and Yu Duan. "Analysis of the effect of graphene, metal, and metal oxide transparent electrodes on the performance of organic optoelectronic devices." Nanomaterials 13, (2022): 25.

[2] K. K. Singha, P. P. Singh, R. Narzary, A. Mondal, M. Gupta, V. G. Sathe, D. Kumar, and S. K. Srivastava. "Crystal structure, Raman spectroscopy and optical property study of Mg-doped SnO2 compounds for optoelectronic devices." Crystals 13, (2023): 932.

[3] S. Sankar and M. T. Ramesan. "Thermal, optical and temperature-dependent electrical properties of poly (aniline-co-pyrrole)/copper alumina nanocomposites for optoelectronic devices." Journal of Thermal Analysis and Calorimetry 147, (2022): 13375-13387.

[4] P. Philipp, Khanh Q. Ngo, John Kieffer, and Tom Wirtz. "Silver diffusion in organic optoelectronic devices: deposition-related processes versus secondary ion mass spectrometry analysis artifacts." The Journal of Physical Chemistry C 119, (2015): 23334-23341.

[5] M. E. Sanchez-Vergara, Leon Hamui, Elizabeth Gómez, Guillermo M. Chans, and José Miguel Galván-Hidalgo. "Design of promising heptacoordinated organotin (IV) complexes-PEDOT: PSS-based composite for new-generation optoelectronic devices applications." Polymers 13, (2021): 1023.

[6] J. Shi, Jiaye Zhang, Lu Yang, Mei Qu, Dong-Chen Qi, and Kelvin HL Zhang. "Wide bandgap oxide semiconductors: from materials physics to optoelectronic devices." Advanced materials 33, (2021): 2006230.

[7] Y. Ma, Yuan Qin, Matthew Porter, Joseph Spencer, Zhonghao Du, Ming Xiao, Boyan Wang et al. "Wide-bandgap nickel oxide with tunable acceptor concentration for multidimensional power devices." Advanced Electronic Materials (2023): 2300662.

[8] P. Gayathri, T. Akila, G. Alan Sibu, Manickam Selvaraj, Mohammed A. Assiri, and V. Balasubramani. "Enhancing photovoltaic applications through precipitating agents in ITO/CIS/CeO_2/Al heterojunction solar cell." Inorganic Chemistry Communications 168 (2024): 112866.

[9] Mastellone, Matteo, Maria Lucia Pace, Mariangela Curcio, Nicola Caggiano, Angela De Bonis, Roberto Teghil, Patrizia Dolce et al. "LIPSS applied to wide bandgap semiconductors and dielectrics: Assessment and future perspectives." Materials 15, no. 4 (2022): 1378.

[10] R. Marnadu, Chandrasekaran, J., Maruthamuthu, S., Vivek, P., Balasubramani, V., & Balraju, P. (2019). Jet Nebulizer Sprayed WO_3-Nanoplate Arrays for High-Photoresponsivity Based Metal–Insulator–Semiconductor Structured Schottky Barrier Diodes. Journal of Inorganic and Organometallic Polymers and Materials, 30, 731–748.

[11] P. Vidhya, Shanmugasundaram, P. Thirunavukkarasu, T. Govindaraj, V. Balasubramani, B. Yogeswari, and M. Karuppusamy. "Enhancement of optoelectronic properties of PbS thin films grown by JNSPtechnique for photodetector applications: an impact of substrate temperature." Journal of Materials Science: Materials in Electronics 34, (2023): 1023.

[12] V. Jagadeesan, R. Sakthivel, and S. Shanmuga Priya. "Improved design and development of an automated JNSPsystem for Ag/Zn: CuO/Si structured diode application." Materials Today: Proceedings (2023).

[13] T. A. Rodrigues, Francisco Werley Cipriano Farias, Julian A. Avila, Emad Maawad, Norbert Schell, Telmo G. Santos, and J. P. Oliveira. "Effect of heat treatments on Inconel 625 fabricated by wire and arc additive manufacturing: an in-situ synchrotron X-ray diffraction analysis." Science and Technology of Welding and Joining 28, (2023): 534-539.

[14] J. Xiao, Yougui Song, and Yue Li. "Comparison of quantitative X-ray diffraction mineral analysis methods." Minerals 13, (2023): 566.

[15] A.K. Abass, "Synthesis of CdTiO3 thin films and study the impact of annealing temperature on their optical, morphological and structural properties." Eurasian J. Anal. Chem. 13 (2018): 5.

[16] H. A. Gatea, Rajaa K. Mohammad, and Sarah M. Khalil. "Impact of annealing temperature on optical properties of CeO2 thin films deposition by spin coating technique." In 2022 International Congress on Human-Computer Interaction, Optimization and Robotic Applications (HORA), pp. 1-3. IEEE, 2022.

[17] M. Justin Paul, R. Suresh, P. Gayathri, V. Balasubramani, Khalid Mashay Al-Anazi, and Mohammad Abul Farah. "CuO-La2O3 Composite-Enabled MIS Schottky Barrier Diodes: A Novel Approach to Optoelectronic Device Diversification." Journal of Inorganic and Organometallic Polymers and Materials (2024): 1-13.

[18] M. Justin Paul, R. Suresh, G. Alan Sibu, V. Balasubramani, and Suganthi Muthusamy. "CuO nanoflowers: Multifaceted implications of various precipitating agents on rectification behaviour." Optical Materials 152 (2024): 115517.

[19] N. Jhansi, D. Balasubramanian, Jih-Hsing Chang, K. Mohanraj, R. Marnadu, M. Aslam Manthrammel, and Mohd Shkir. "Impact of substrate temperature on structural, electric and optical characteristics of CuO thin films grown by JNS pyrolysis technique." Silicon (2022): 1-11.

[20] M. Khammar, F. Ynineb, S. Guitouni, Y. Bouznit, and N. Attaf. "Crystallite size and intrinsic strain contribution in band gap energy redshift of ultrasonic-sprayed kesterite CZTS nanostructured thin films." Applied Physics A 126, (2020): 398.

[21] A. Nejad, Xiang Li, Tianxin Zhu, Yun Liu, and Chuanxi Duan. "Mid-infrared Laser Spectroscopy of Jet-Cooled Formic Acid Trimer: Mode-Dependent Line Broadening in the C–O Stretching Region." The Journal of Physical Chemistry Letters 14, (2023): 7795-7801.

[22] S. Kanazawa, Yasuhiro Yamada, and Satoshi Sato. "Infrared spectroscopy of graphene nanoribbons and aromatic compounds with sp 3 C–H (methyl or methylene groups)." Journal of Materials Science 56 (2021): 12285-12314.

[23] D. Hurova, E., V. G. Geidarov, I. S. Braude, N. A. Aksenova, S. G. Stepanian, L. Adamowicz, and N. N. Galtsov. "Structural studies of amorphous polymer films: Experiment and calculation." Low Temperature Physics 50, (2024): 272-278.

[24] R. M. German, "Coarsening in sintering: grain shape distribution, grain size distribution, and grain growth kinetics in solid-pore systems." Critical reviews in solid state and materials sciences 35, (2010): 263-305.

[25] M. R. Rokni, S. R. Nutt, C. A. Widener, V. K. Champagne, and R. H. Hrabe. "Review of relationship between particle deformation, coating microstructure, and properties in high-pressure cold spray." Journal of thermal spray technology 26 (2017): 1308-1355.

[26] A. P. Vink, A. Meijerink, and G. D. Jones. "Temperature dependence of infrared-absorption lines of Co 2+ in cadmium halides." Physical Review B 66, (2002): 134303.

[27] S. V. Syrotyuk, and O. P. Malyk. "Effect of the Spin-orbit Interaction on the Electronic Band Energies in Cadmium Chalcogenides Evaluated within the HSE06-GW Approach." (2021).

[28] U. Diebold and T. E. Madey. "TiO2 by XPS." Surface Science Spectra 4, (1996): 227-231.

[29] N. M. Khusayfan, Atef Fayez Qasrawi, Hazem K. Khanfar, and Seham R. Alharbi. "Lead selenide thin films designed for laser sensing and visible light communications." Silicon 15, (2023): 6971-6979.

[30] M. Temiz and S. Çelik. "Influence of growth temperature on the structural and optical characteristics of PbZnS thin films." Chalcogenide Letters 21, (2024): 867-872.

[31] A. M. Hassanien, A. A. A. Darwish, A. M. Kamal, Mahmoud Al-Gawati, and Taymour A. Hamdalla. "Annealing effect on the morphology, linear and non-linear optical properties of squaraine derivative thin films for optoelectronics applications." Optical Materials 142 (2023): 114033.

[32] Katrapally Vijaya kumar, and Sara Durga Bhavani. "Effect of Calcination Temperature on Structural and Optical Properties of Nickel Aluminate Nanoparticles." East European Journal of Physics 3 (2023): 355-362.

[33] Lana Omar Ahamed, Niyazi Bulut, Fatih Osmanlıoğlu, Beyhan Tatar, Hanifi Kebiroglu, Tankut Ates, Suleyman Koytepe, Burhan Ates, Serhat Keser, and Omer Kaygili. "Theoretical and experimental investigation of the effects of Pr dopant on the electronic band structure, thermal, structural, in vitro biocompatibility of Er-based hydroxyapatites." Journal of Molecular Structure 1280 (2023): 135095.

[35] Jingyun Hu, Yiwei Zhang, and Xinping Zhang. "Low-Temperature Discrimination of Defect States by Exciton Dynamics in Thin-Film MAPbBr3 Perovskite." The Journal of Physical Chemistry Letters 13, (2022): 6093-6100.

[36] N. Rani, Goswami, B., & Ahlawat, R. (2022). Impact of Annealing on Structure, Morphology, Bandgap, Optical and Dielectric Behavior of Er3+ Doped SiO2 Nanopowder Useful for Photonic Devices. Silicon, 14, 8543–8555.

[37] H. E. Doghmane, Challali, F., Touam, T., Chelouche, A., & Djouadi, D. (2021). Radio Frequency Magnetron Sputtering Growth of Titanium Dioxide Thin Films: Effects of Substrate Temperature on Microstructural and Optical Properties. Journal of Nano Research, 70, 1–14.

[38] M. Alsharif, Alqurashi, R. S., & Hamdalla, T. (2024). The role of annealing in optimizing the electrical, linear, and nonlinear optical properties ZIf-8@TiO2 films for possible use in photonic and optoelectronic devices. Physica Scripta, 99.

[39] G. Alan Sibu, P. Gayathri, T. Akila, R. Marnadu, and V. Balasubramani. "Manifestation on the choice of a suitable combination of MIS for proficient Schottky diodes for optoelectronics applications: A comprehensive review." Nano Energy (2024): 109534.

[40] T. Akila, P. Gayathri, G. Alan Sibu, V. Balasubramani, Hamad Al-Lohedan, and Dhaifallah M. Al-Dhayan. "Augmented photovoltaic performance of Cu/Ce-(Sn: Cd)/n-Si Schottky barrier diode utilizing dual-doped Ce-(Sn: Cd) thin films." Optical Materials 149 (2024): 115133.

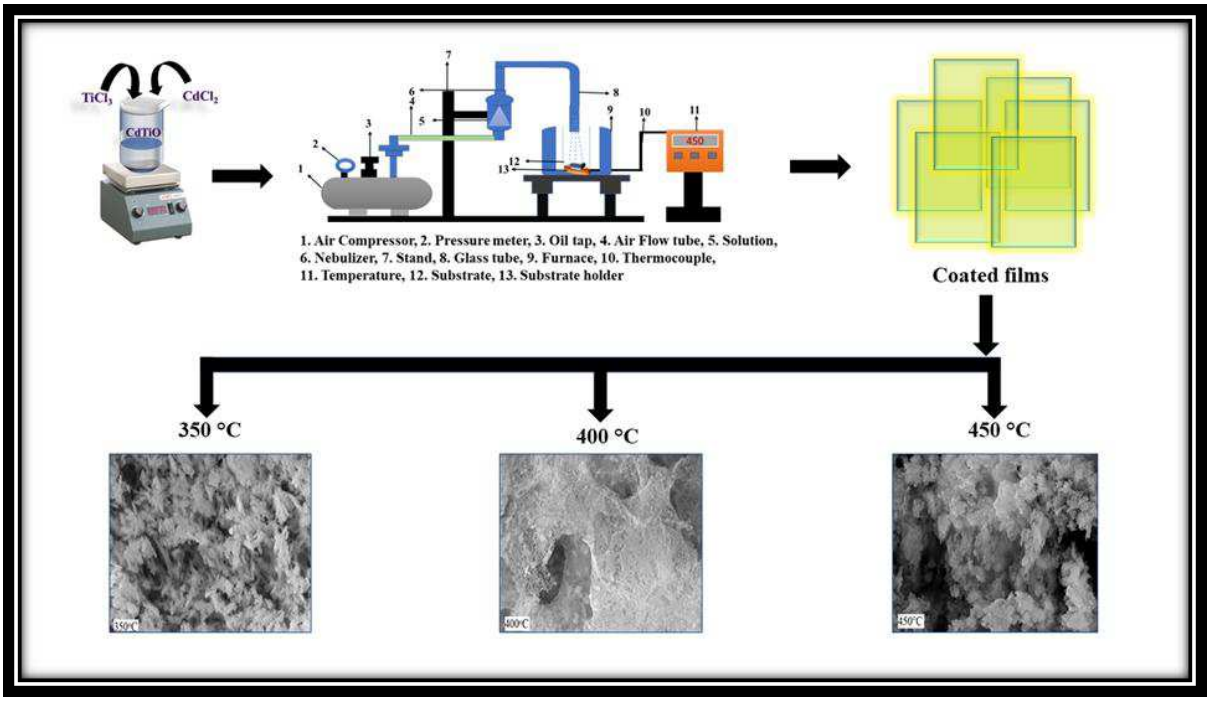


Fig. 1. Schematic representation of the preparation of $CdTiO_3$ thin films.

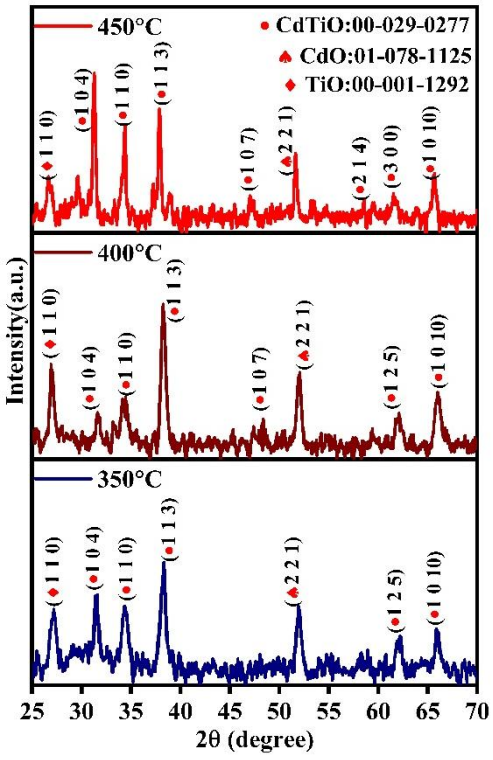


Fig. 2. X-ray diffraction patterns of $CdTiO_3$ thin films for different temperatures**.**

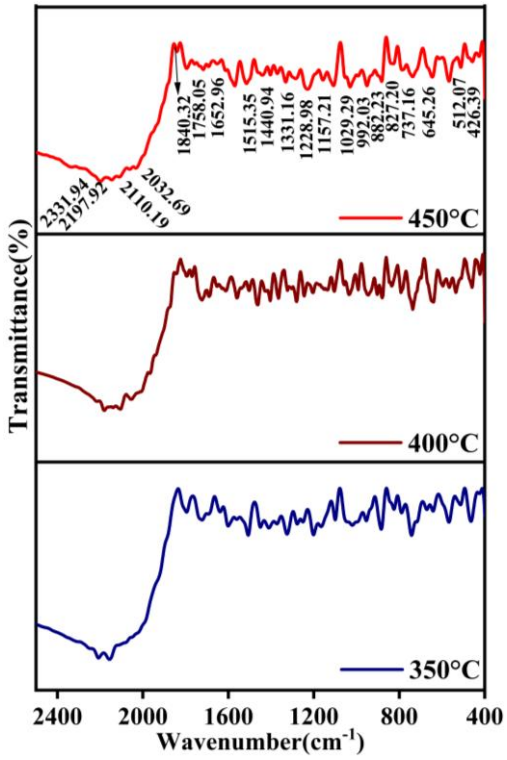


Fig. 3. FTIR spectra of $CdTiO_3$ thin films for different temperatures**.**

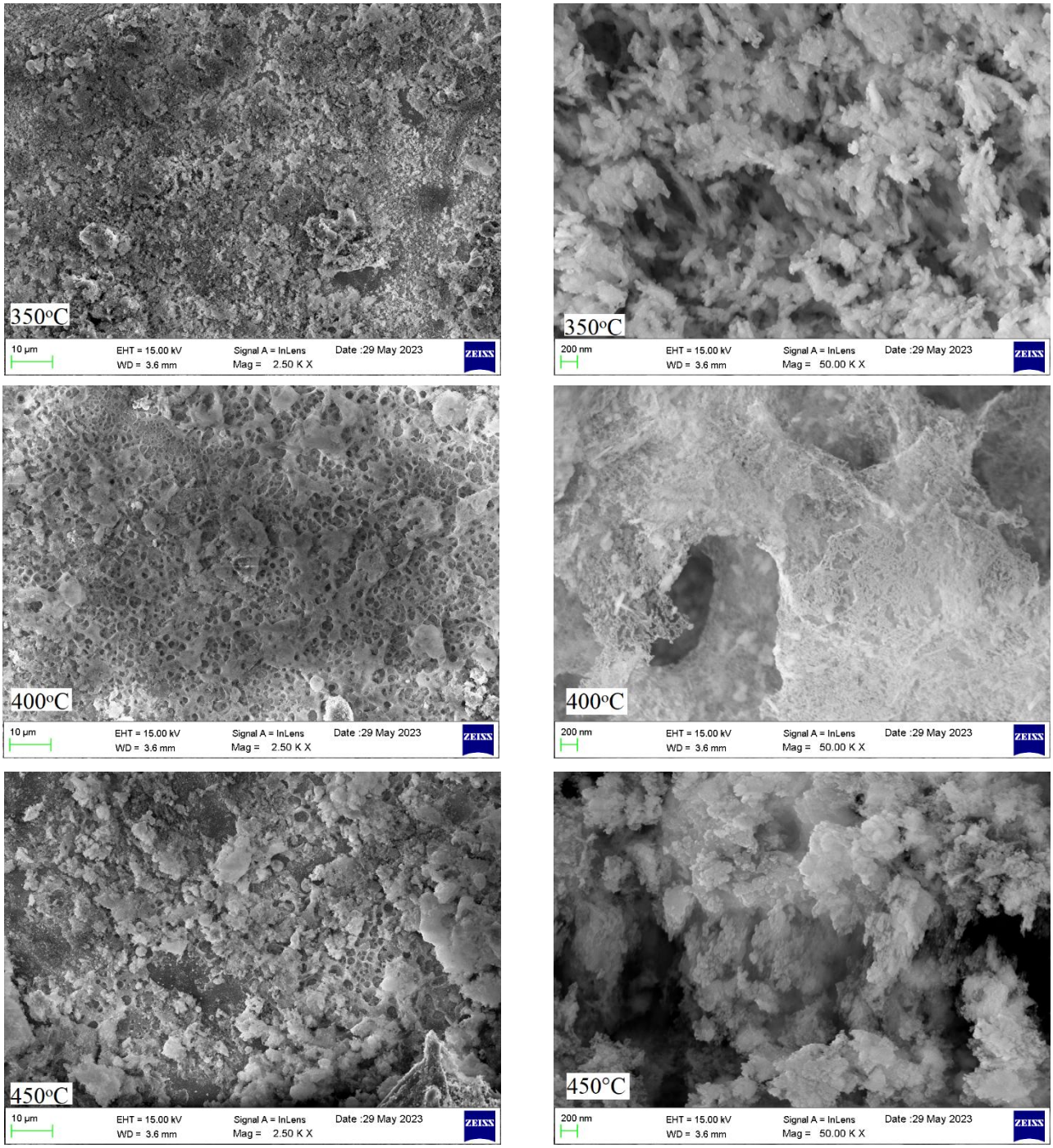
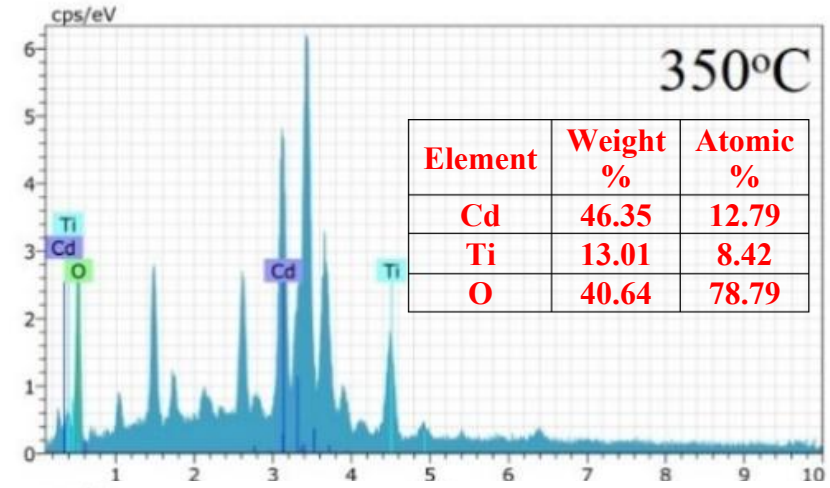
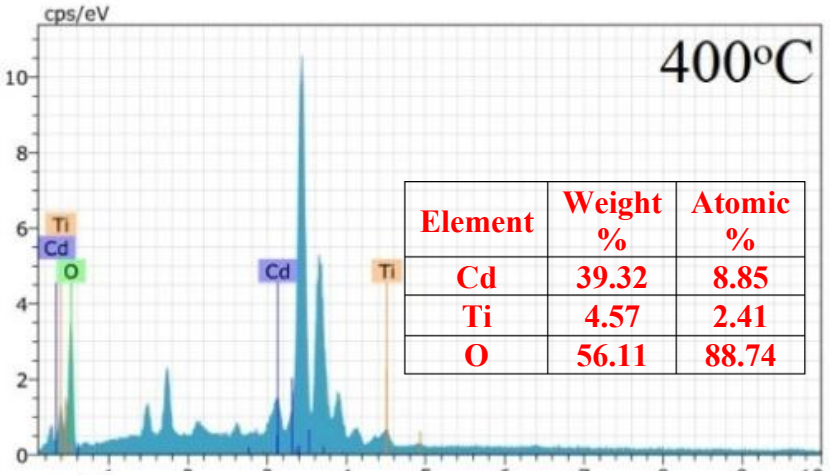


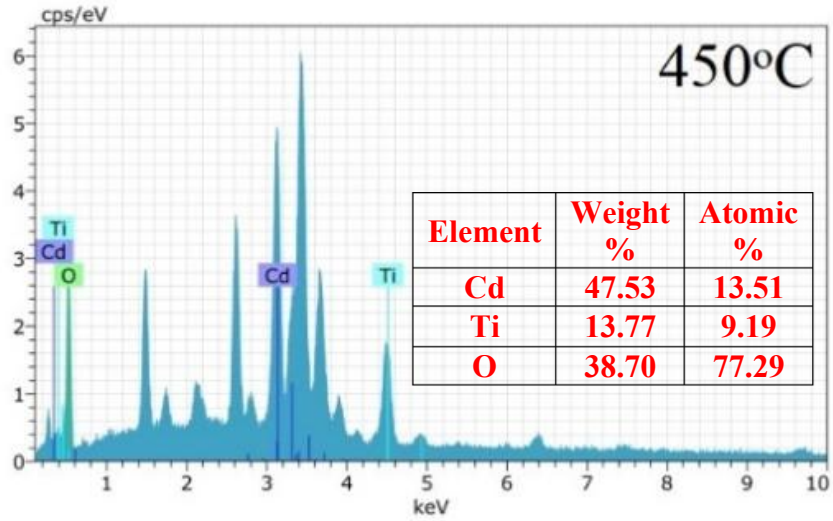
Fig. 4. FE-SEM images of $CdTiO_3$ thin films for different temperatures**.**



Element	Weight %	Atomic %
Cd	46.35	12.79
Ti	13.01	8.42
O	40.64	78.79

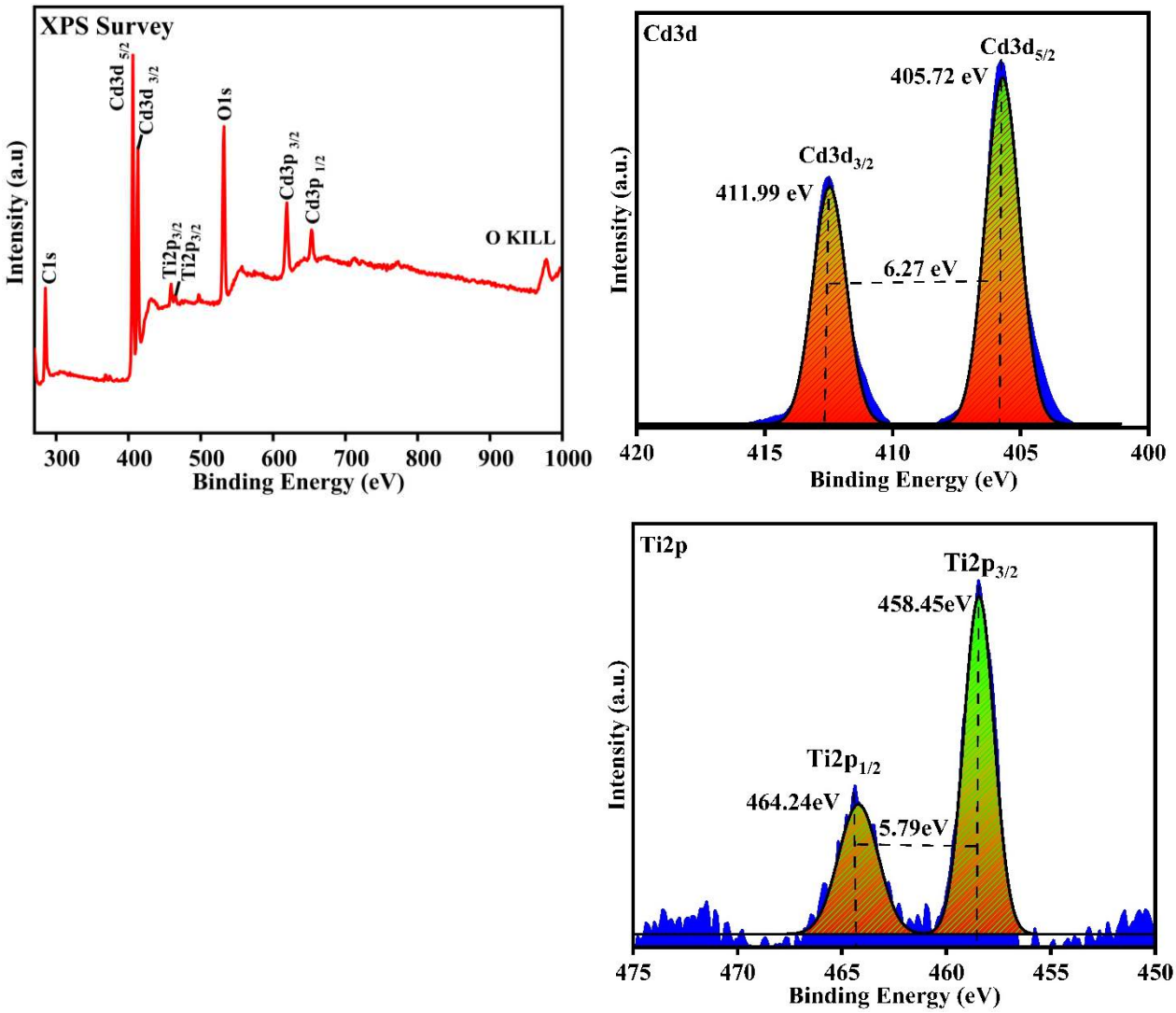


Element	Weight %	Atomic %
Cd	39.32	8.85
Ti	4.57	2.41
O	56.11	88.74



Element	Weight %	Atomic %
Cd	47.53	13.51
Ti	13.77	9.19
O	38.70	77.29

Fig. 5. EDAX Spectra of $CdTiO_3$ thin films for different temperatures.



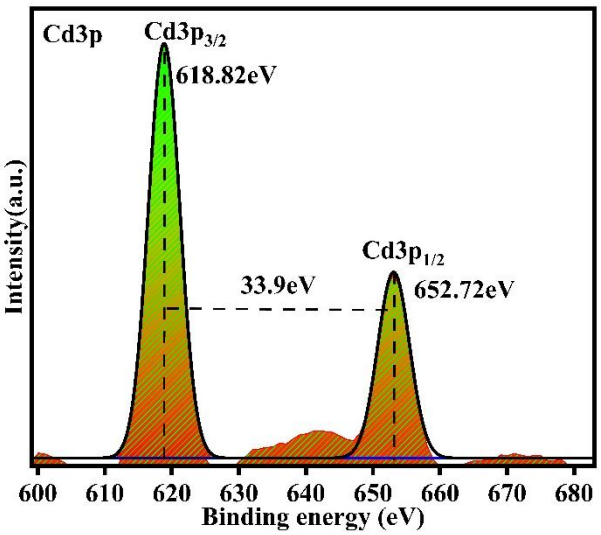
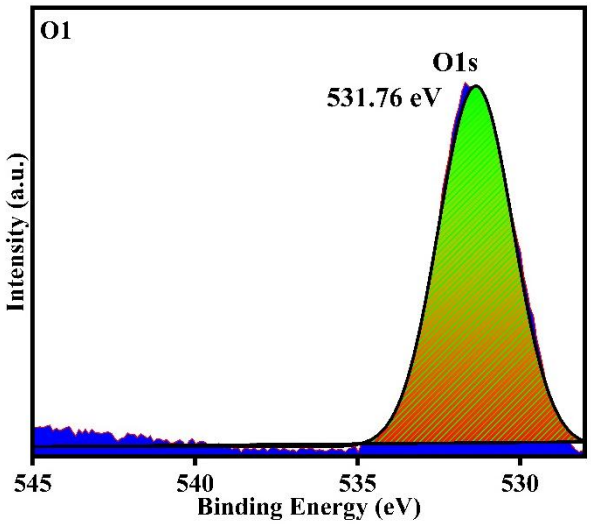


Fig. 6. XPS spectra of $CdTiO_3$ film at 450 ^oC temperatures.



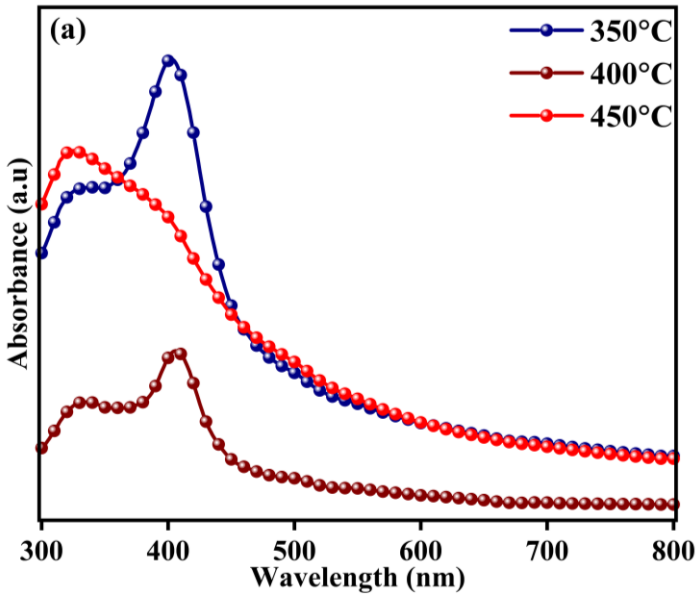


Fig. 7. Absorbance spectra of $CdTiO_3$ thin films for different temperatures.

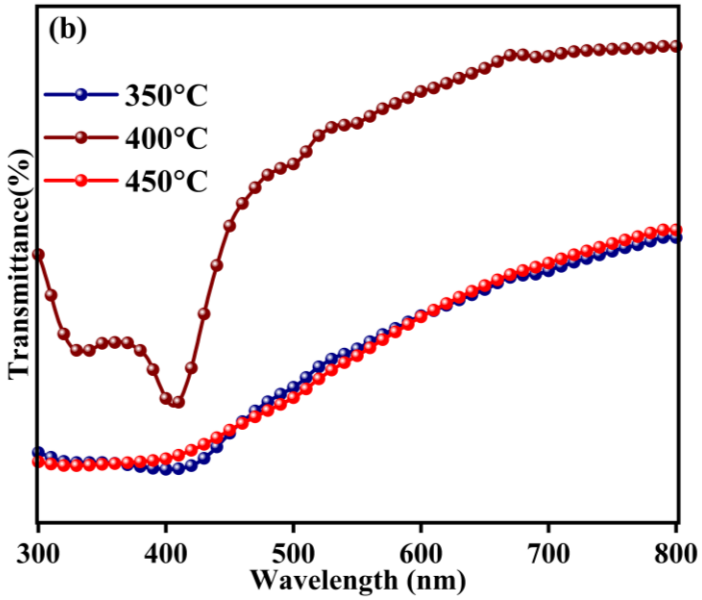


Fig. 8. Transmittance spectra of $CdTiO_3$ thin films for different temperatures.

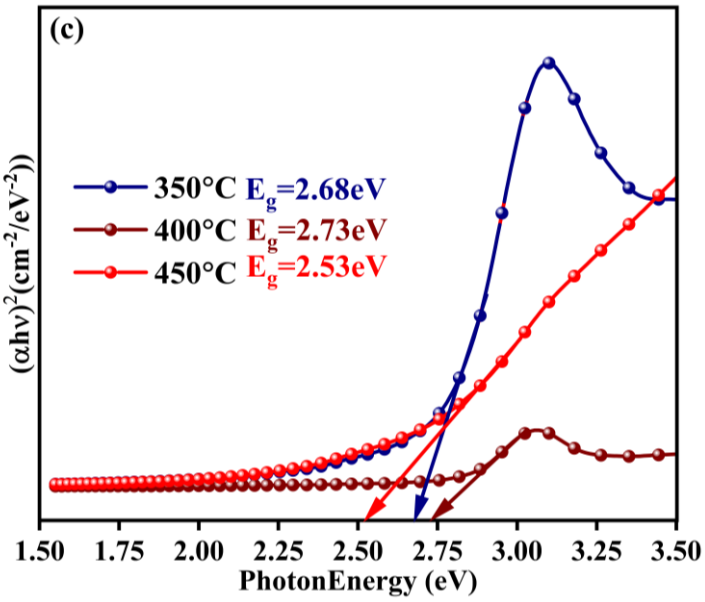


Fig. 9. The dependence of $(\alpha h\upsilon)^2$ on $h\upsilon$ for $CdTiO_3$ thin films for different temperatures.

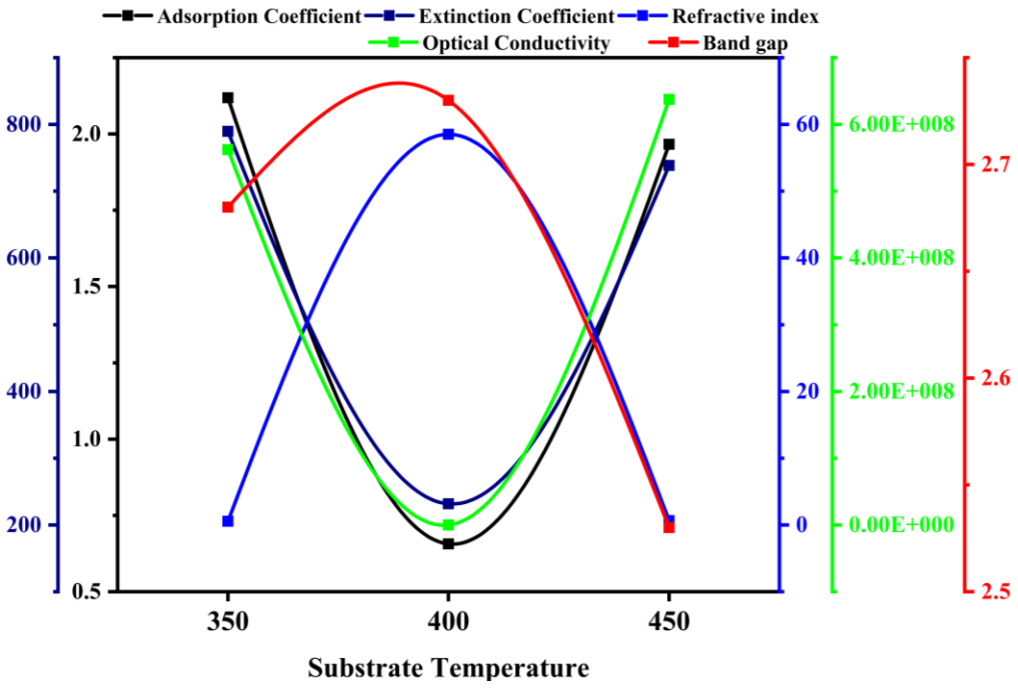


Fig. 10. Optical parameters vs different temperatures for $CdTiO_3$ thin films.

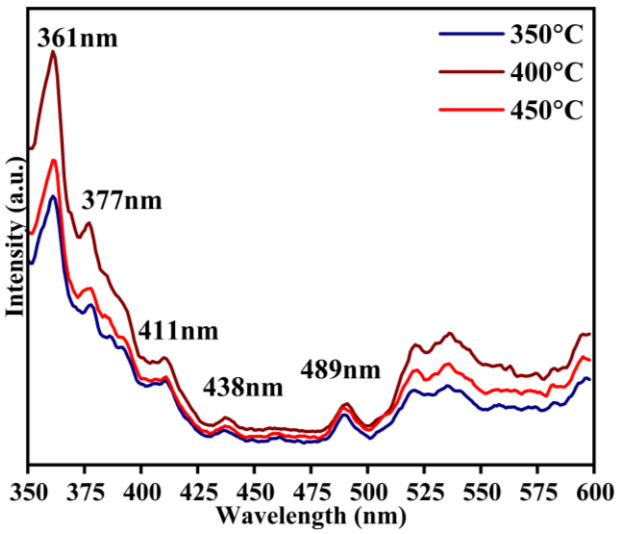


Fig. 11. Photoluminescence spectra of $CdTiO_3$ thin films for different temperatures.

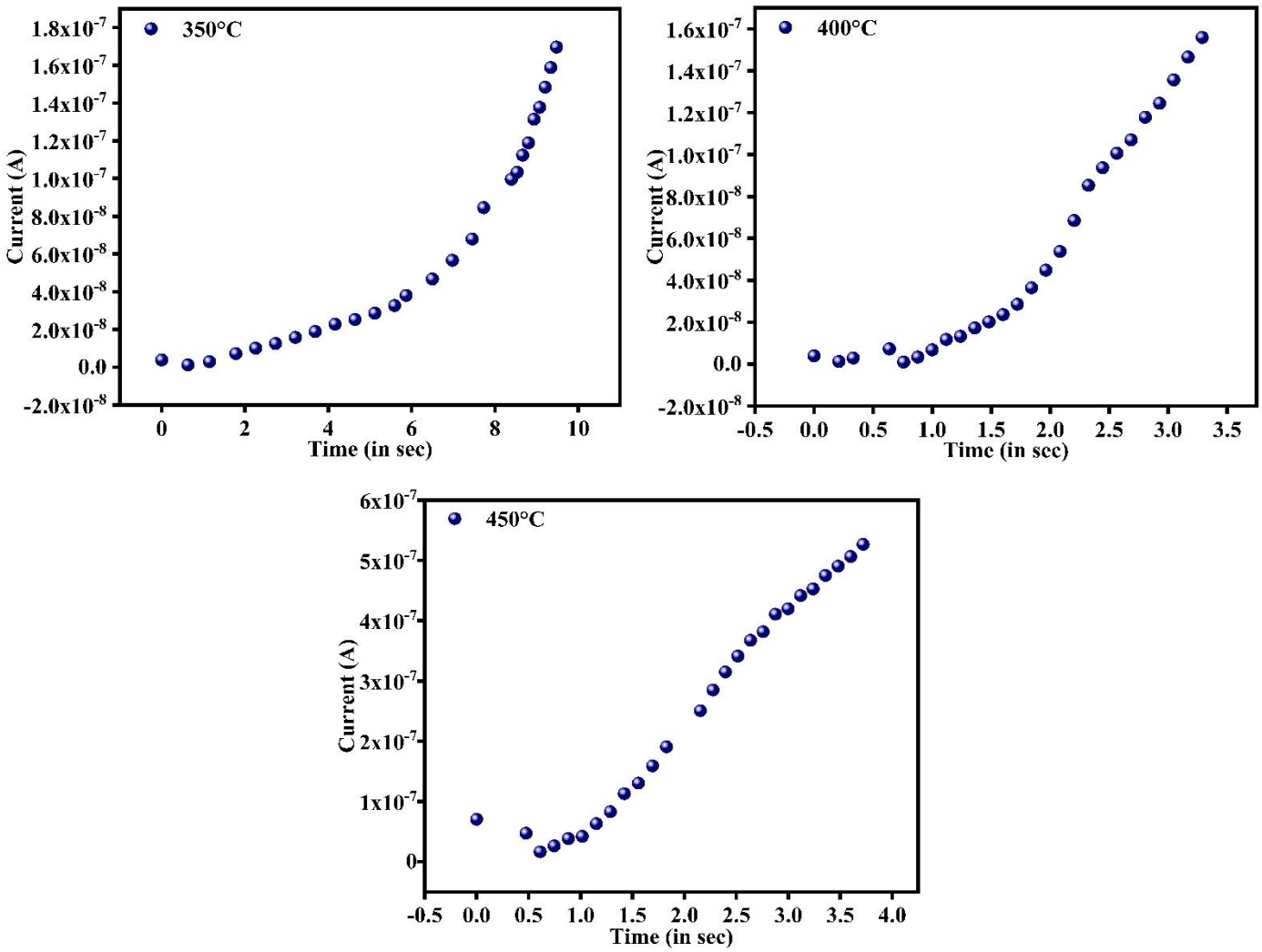


Fig. 12. Photocurrent of $CdTiO_3$ thin films for different temperatures.

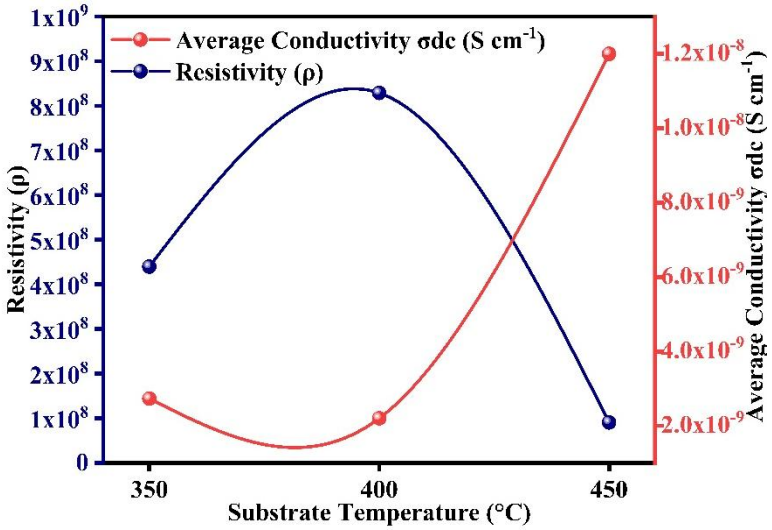


Fig. 13. Electrical Conductivity of $CdTiO_3$ thin films for different temperatures.

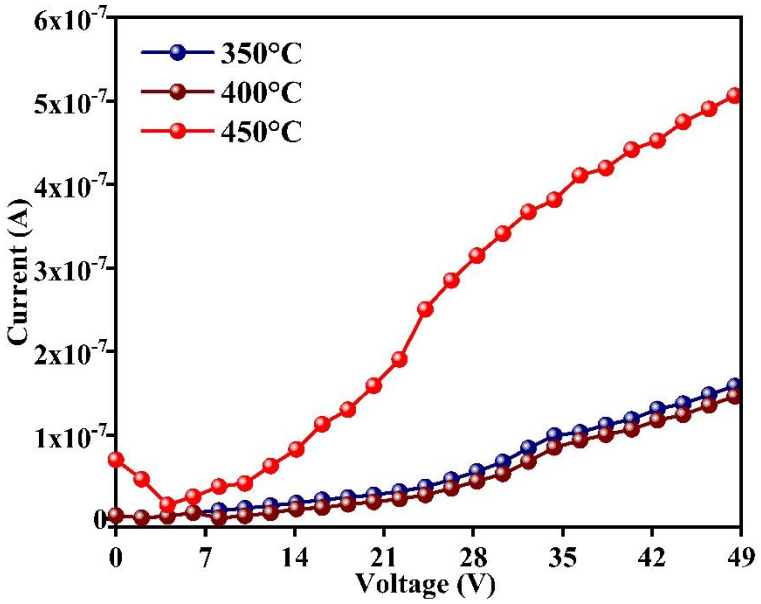


Fig. 14. Current vs voltage plot of the $CdTiO_3$ thin films using dc electrical conductivity.

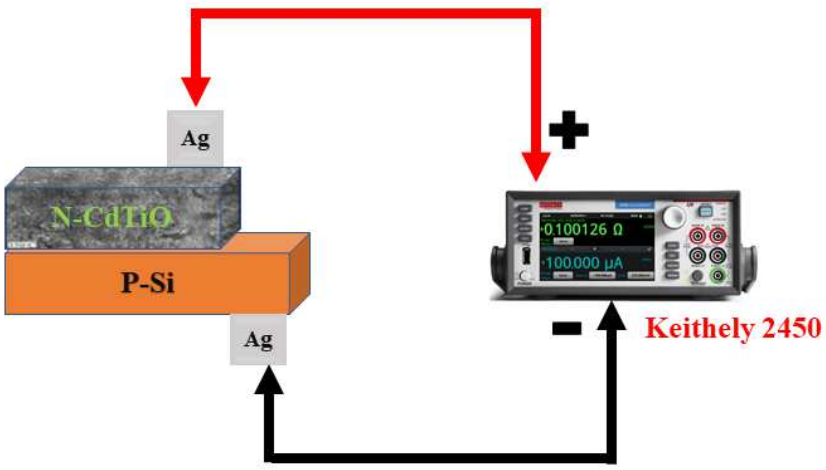


Fig. 15. Schematic representation of $CdTiO_3$/P-Si Photodiode structure

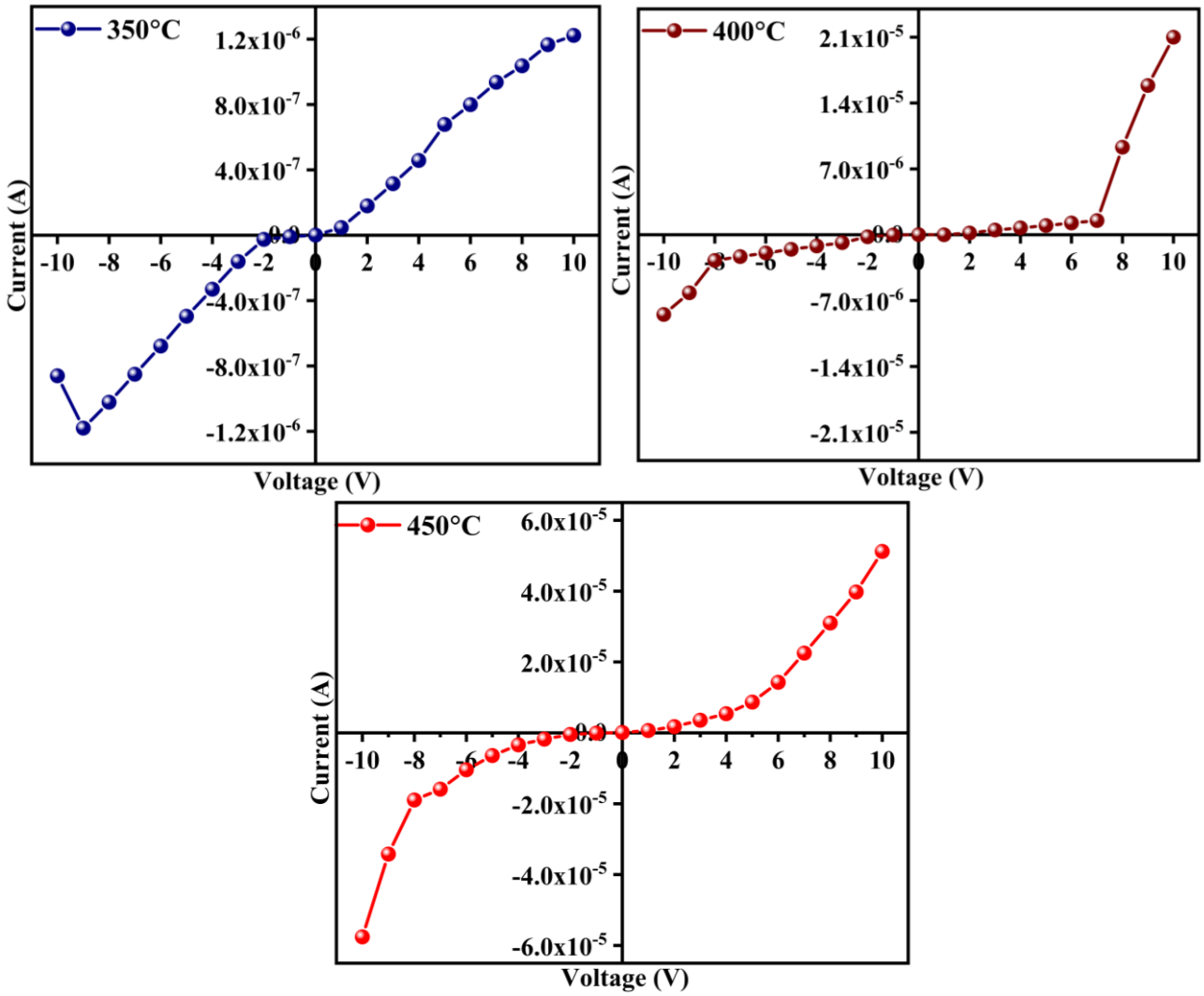


Fig. 16. J–V plot for pure $CdTiO_3$ /p-Si Photodiode.

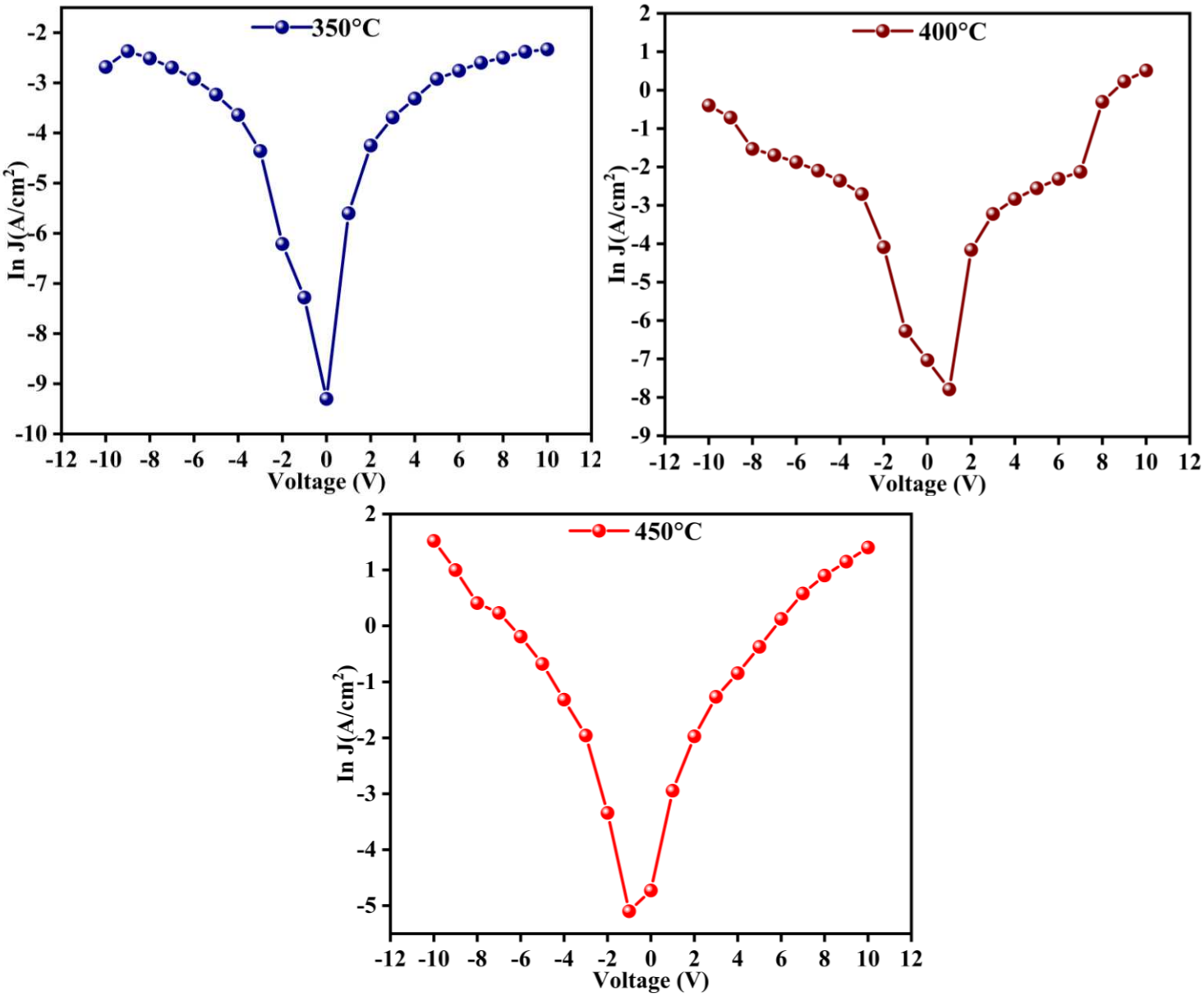


Fig. 17. The forward and reverse-bias ln(J)-V characteristics of pure $CdTiO_3$ /p-Si Photodiode.

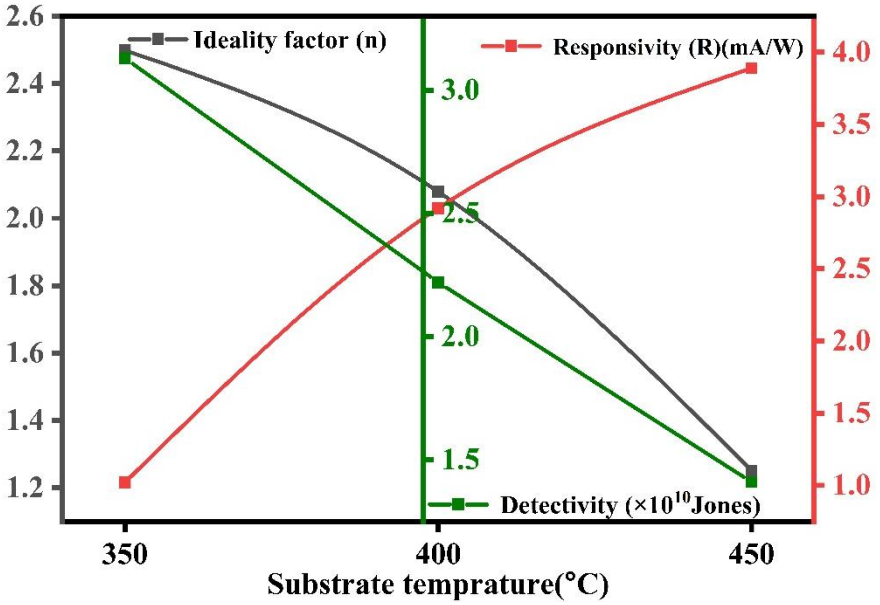


Fig. 18. The Photodiode properties of pure $CdTiO_3$ /p-Si Photodiode.

Supplementary Files

This is a list of supplementary files associated with this preprint. Click to download.

- TableCdTiO.docx